

Bremsstrahlung polarization correlations and their application for polarimetry of electron beamsS. Tashenov,¹ T. Bäck,² R. Barday,³ B. Cederwall,² J. Enders,³ A. Khaplanov,² Yu. Fritzsche,³ K.-U. Schässburger,² A. Surzhykov,^{1,4} V. A. Yerokhin,^{1,4,5} and D. Jakobassa-Amundsen⁶¹*Physikalisches Institut der Universität Heidelberg, 69120 Heidelberg, Germany*²*Royal Institute of Technology, SE-10691 Stockholm, Sweden*³*Institut für Kernphysik, Technische Universität Darmstadt, 64289 Darmstadt, Germany*⁴*GSI Helmholtzzentrum für Schwerionenforschung GmbH, 64291 Darmstadt, Germany*⁵*Center for Advanced Studies, St. Petersburg State Polytechnical University, Polytekhnicheskaya 29, St. Petersburg 195251, Russia*⁶*Mathematics Institute, University of Munich, Theresienstrasse 39, 80333 Munich, Germany*

(Received 5 November 2012; published 19 February 2013)

Linear polarization of hard x rays emitted in the process of atomic-field electron bremsstrahlung has been measured with a polarized electron beam. The correlation between the initial orientation of the electron spin and the angle of photon polarization has been systematically studied by means of Compton and Rayleigh polarimetry techniques applied to a segmented germanium detector. The results are in good agreement with those of fully relativistic calculations. The observed correlations are also explained classically and in a unique way manifest that due to the spin-orbit interaction the electron scattering trajectory is not confined to a single scattering plane. The developed photon polarimetry technique with a passive scatterer is very efficient and accurate and thus allows for additional applications. Bremsstrahlung polarization correlations lead to an alternative method of polarimetry of electron beams. Such a method is sensitive to all three components of the electron spin. It can be applied in a broad range of the electron beam energies from ≈ 100 keV up to a few tens of MeV. The results of a measurement at 100 keV are shown. The optimum scheme for electron polarimetry is analyzed and the relevant theoretical predictions are presented.

DOI: [10.1103/PhysRevA.87.022707](https://doi.org/10.1103/PhysRevA.87.022707)

PACS number(s): 34.80.Nz, 41.60.-m, 32.80.Fb

I. INTRODUCTION

Radiation spectra in relativistic electron-atom collisions are dominated by atomic-field bremsstrahlung. Bremsstrahlung is one of the fundamental ways in which the electromagnetic field interacts with matter. It occurs for every charged particle moving through matter, and most of its properties are understood classically. For this reason it was used for many decades to study dynamics of colliding particles. In the earlier days research focused on the spectral shapes and the angular distributions of the emitted photons [1–7]. They are now well understood and the theoretical predictions are published in the form of tables [8–10]. Accurate measurements of the cross sections are still occasionally made [11–13].

Photon polarization was also closely examined both theoretically [14–17] and experimentally [18–21]. It reveals the fine details of the scattered electron dynamics and in particular the influence of its spin [22,23]. Here one takes a particular interest in the dynamics because of the extremely strong fields experienced by the electron. In these fields the relativistic and the spin effects become pronounced. In particular the magnetic field induced by the nucleus in the electron's rest frame is strong enough to cause a significant interaction with the spin—the spin-orbit interaction. It is significant even for a single-electron path near the nucleus. Therefore such a free-free electron radiative transition can be used to study the nature of the spin-orbit interaction.

The spin-orbit interaction in the relativistic regime contributes significantly to the deflection of the scattered electron. In the case when the spin is oriented perpendicular to the scattering plane it causes Mott scattering asymmetry [24,25]. Similarly, due to forward character of the photon emission at relativistic energies, it causes the spin asymmetry of

bremsstrahlung emission. This effect is now well understood theoretically [26–30] as well as experimentally [31–35]. Furthermore, detailed experimental data were also obtained for more differential studies in which the scattered electrons were observed [36–38]. In some of these studies linear photon polarization was observed too [39,40]. However, until recently in no experiment were the polarizations of both the electron and the photon controlled at the same time.

One such experiment was performed by our group [22]. We demonstrated that for longitudinally polarized electrons the spin-orbit interaction rotates the plane of the electron scattering. The rotation of the scattering plane can be unambiguously observed in the polarization of the emitted photons. The angle of linear polarization is defined by the electron acceleration direction. For a spinless electron it should point towards the scattering center—the nucleus and thus it should be confined to the scattering plane. We saw that the direction of the acceleration is not confined to the reaction plane—the plane defined by the incoming electron and the photon. This uniquely identifies that the electron trajectory is not confined to a single scattering plane.

Furthermore, since bremsstrahlung at the hard-photon end of the spectrum can be considered as a time reversal of photoionization [41–43], this effect corresponds to production of longitudinally polarized electrons by photoionization of unpolarized atoms with linearly polarized photons, i.e., by photons with no preferred spin orientation. It was already known that photoionization may produce longitudinally polarized electrons via the Fano effect [44]. However, it requires spin-oriented photons, i.e., circularly polarized light. On the other hand, the production of longitudinally polarized electrons with linearly polarized light is a different phenomenon. Its

underlying physics is significantly different from that of the Fano effect. In contrast to the Fano effect it requires strong fields and relativistic energies.

In this article we further describe these phenomena. We provide a complete account of the experimental details omitted in the Letter [22] and add the observation of the rotation of bremsstrahlung polarization caused by transversely polarized electrons. An experiment performed by another group also focused on the influence of the transverse spin [23]. They have identified that the angle of photon polarization does not depend on its energy. In this article we will interpret this phenomenon. These correlations were predicted long ago [16,45–49], but only recently have the experimental techniques become sensitive enough to observe them. We explain these correlations classically. We show that a number of them are parity forbidden. With a test measurement we demonstrate that they can be applied for polarimetry of relativistic electron beams.

II. DEFINITIONS OF POLARIZATION CORRELATIONS

The geometry of bremsstrahlung is shown in Fig. 1(a). Each component of the electron spin may potentially influence the intensity and polarization of the emitted photon. Two equivalent notations are adopted to describe these correlations. The first notation uses the correlation coefficients C_{kl} in the terminology of Tseng and Pratt [46]; see Table I. The second

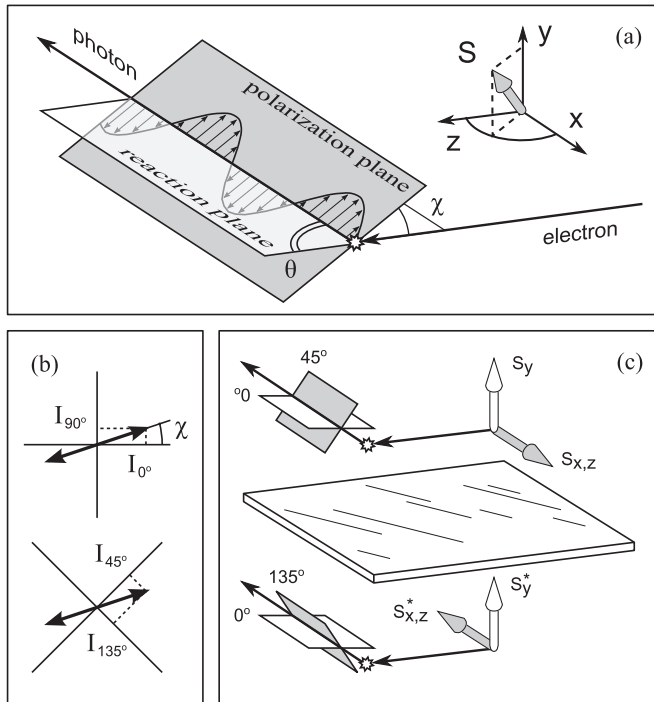


FIG. 1. (a) Bremsstrahlung geometry. The incoming electron moves along the \hat{z} axis. The reaction plane, defined by the incoming electron and the emitted photon directions, coincides with the (x,z) plane. The photons are emitted at the angle θ with respect to \hat{z} . The photon polarization plane is tilted by an angle χ with respect to the reaction plane. (b) Intensities of light polarized within planes tilted by 0° , 45° , 90° , and 135° . (c) Transformation of planes, vectors, and axial vectors in mirror reflection.

TABLE I. Notation for electron and photon polarization for correlation parameters C_{kl} in the terminology of Tseng and Pratt [46].

k	Electron	l	Photon
0	Unpolarized	0	$d\sigma$, total
1	\hat{x} , transverse within the reaction plane	1	P_2 , linear
2	\hat{y} , transverse perp. to the reaction plane	2	P_3 , circular
3	\hat{z} , longitudinal	3	P_1 , linear

notation uses the Stokes parameters $P_n(x,y,z)$ as a function of the electron spin orientation (x,y,z) , in the terminology of Yerokhin and Surzhykov [48]. Here the \hat{z} axis is along the incoming electron beam direction, and (x,z) is the photon emission plane. The Stokes parameters P_1 and P_2 are defined in the following way:

$$P_1 = \frac{I_{0^\circ} - I_{90^\circ}}{I_{0^\circ} + I_{90^\circ}}, \quad P_2 = \frac{I_{45^\circ} - I_{135^\circ}}{I_{45^\circ} + I_{135^\circ}}, \quad (1)$$

where I_φ is the number of photons polarized in the plane tilted by the angle φ with respect to the reaction plane (x,z) ; see Fig. 1(b). The degree P and the angle χ of photon linear polarization are related to P_1 and P_2 as

$$P = \sqrt{P_1^2 + P_2^2}, \quad \cos 2\chi = \frac{P_1}{P}, \quad \sin 2\chi = \frac{P_2}{P}. \quad (2)$$

There are 12 possible correlations involving the orientation of the electron spin and the direction and linear polarization of the emitted photon. However some of them are parity forbidden. To prove this we describe the parity transformation as a mirror reflection and a rotation. The mirror reflection does not affect the photons linearly polarized within the reflection plane, in our case the reaction plane (x,z) , i.e., $P_1 \Rightarrow P_1$; see Fig. 1(c). However, it changes the sign of photon polarization within the plane turned by 45° with respect to the reflection plane, i.e., $P_2 \Rightarrow -P_2$. The electron spin is an axial vector. Therefore with respect to the mirror reflection it transforms as a vector and in addition it changes sign, i.e., the spin components are transformed as $(x,y,z) \Rightarrow (-x,y,-z)$. The mirror reflection symmetry thus leads to the following rules:

$$\begin{aligned} P_1(1,0,0) &= P_1(-1,0,0), & P_2(1,0,0) &= -P_2(-1,0,0), \\ d\sigma(1,0,0) &= d\sigma(-1,0,0), & P_1(0,1,0) &= P_1(0,1,0), \\ P_2(0,1,0) &= -P_2(0,1,0), & d\sigma(0,1,0) &= d\sigma(0,1,0), \\ P_1(0,0,1) &= P_1(0,0,-1), & P_2(0,0,1) &= -P_2(0,0,-1), \\ d\sigma(0,0,1) &= d\sigma(0,0,-1). \end{aligned}$$

From these equations it follows that

$$d\sigma(0,0,0) = d\sigma(1,0,0) = d\sigma(0,0,1), \quad (3)$$

$$P_1(0,0,0) = P_1(1,0,0) = P_1(0,0,1), \quad (4)$$

$$P_2(0,0,0) = P_2(0,1,0) = 0, \quad (5)$$

or, with the definitions of [46], $C_{10} = C_{30} = C_{01} = C_{21} = C_{13} = C_{33} = 0$. These equations are satisfied as long as parity is conserved. It is conserved in electromagnetic interactions which include bremsstrahlung. However, an admixture of the parity-breaking weak interaction, i.e., a Z-boson exchange, may break these equations. The mirror symmetry does not

affect other polarization correlations which are in a general case indeed not equal to zero [46–49]:

$$C_{00} = d\sigma(0,0,0), \quad (6)$$

$$C_{03} = P_1(0,0,0), \quad (7)$$

$$C_{11} = -P_2(1,0,0), \quad (8)$$

$$C_{23} = P_1(0,0,0) - P_1(0,1,0), \quad (9)$$

$$C_{31} = P_2(0,0,1), \quad (10)$$

$$C_{20} = 1 - \frac{d\sigma(0,1,0)}{d\sigma(0,0,0)}. \quad (11)$$

III. POLARIZATION CORRELATIONS FOR ARBITRARY POLARIZED ELECTRONS

In order to derive the photon intensity and Stokes parameters for an *arbitrary* polarization of the electron beam, it is natural to employ the density matrix approach. Within such an approach, analysis of the bremsstrahlung process can be traced back to the photon spin-density matrix [48]:

$$\begin{aligned} \langle \mathbf{k}\lambda | \hat{\rho}_\gamma | \mathbf{k}'\lambda' \rangle &= \sum_{m_i, m_i'} \int d\Omega_f \langle \mathbf{p}_i m_i | \boldsymbol{\alpha} \mathbf{u}_\lambda e^{i\mathbf{k}\mathbf{r}} | \mathbf{p}_f m_f \rangle^* \\ &\times \langle \mathbf{p}_i m_i' | \boldsymbol{\alpha} \mathbf{u}_\lambda e^{i\mathbf{k}\mathbf{r}} | \mathbf{p}_f m_f \rangle \langle \mathbf{p}_i m_i | \hat{\rho}_e | \mathbf{p}_i m_i' \rangle, \end{aligned} \quad (12)$$

which is directly related to the polarization parameters P_1 , P_2 , and P_3 as

$$\langle \mathbf{k}\lambda | \hat{\rho}_\gamma | \mathbf{k}'\lambda' \rangle = \frac{1}{2} \text{Tr}(\hat{\rho}_f) \begin{pmatrix} 1 + P_3 & P_1 - iP_2 \\ P_1 + iP_2 & 1 - P_3 \end{pmatrix}, \quad (13)$$

and whose trace over the photon helicity $\lambda = \pm 1$ (i.e., over the spin projection on the momentum \mathbf{k}) is proportional to the intensity of the emitted light. As seen from Eq. (12), the density matrix depends not only on the amplitudes $\langle \mathbf{p}_i m_i | \boldsymbol{\alpha} \mathbf{u}_\lambda e^{i\mathbf{k}\mathbf{r}} | \mathbf{p}_f m_f \rangle$ that describe radiative transition between initial $|\mathbf{p}_i m_i\rangle$ and final $|\mathbf{p}_f m_f\rangle$ continuum-electron states with asymptotic momenta $\mathbf{p}_{i,f}$ and spin projections $m_{i,f} = \pm 1/2$, but also on the polarization of the incident electron beam. Such a polarization is characterized by the electron density matrix $\hat{\rho}_e$ which, rather similarly to the photon case (13), can be parametrized as [50]

$$\hat{\rho}_e = \frac{1}{2}(I + S_x \sigma_x + S_y \sigma_y + S_z \sigma_z), \quad (14)$$

where σ_i , $i = x, y, z$, are the standard Pauli matrices, and S_x , S_y , and S_z are the components of the spin-polarization vector $\mathbf{S} = (S_x, S_y, S_z)$. The absolute value of this vector may vary from $S = \sqrt{S_x^2 + S_y^2 + S_z^2} = 0$ for an unpolarized to $S = 1$ for a completely polarized electron beam.

By inserting expansion (14) into Eq. (12) we find that the density matrix of the emitted photons can be written—in the most general case—as

$$\begin{aligned} \langle \mathbf{k}\lambda | \hat{\rho}_\gamma | \mathbf{k}'\lambda' \rangle &= (1 - S_x - S_y - S_z) \langle \mathbf{k}\lambda | \hat{\rho}_\gamma(0,0,0) | \mathbf{k}'\lambda' \rangle \\ &+ S_x \langle \mathbf{k}\lambda | \hat{\rho}_\gamma(1,0,0) | \mathbf{k}'\lambda' \rangle \\ &+ S_y \langle \mathbf{k}\lambda | \hat{\rho}_\gamma(0,1,0) | \mathbf{k}'\lambda' \rangle \\ &+ S_z \langle \mathbf{k}\lambda | \hat{\rho}_\gamma(0,0,1) | \mathbf{k}'\lambda' \rangle, \end{aligned} \quad (15)$$

where the matrix $\hat{\rho}_\gamma(0,0,0)$ characterizes the bremsstrahlung radiation for the case of an unpolarized incident beam, and $\hat{\rho}_\gamma(1,0,0)$, $\hat{\rho}_\gamma(0,1,0)$, and $\hat{\rho}_\gamma(0,0,1)$ correspond to complete electron polarization in the x , y , and z directions, respectively. Based on expression (15) one can easily calculate all the properties of the bremsstrahlung radiation for an arbitrary electron polarization. For example, the intensity of the emitted photons, which is proportional to the differential (in the energy $E = \hbar ck$ and the photon emission angle) cross section, can be obtained as

$$\begin{aligned} I &\propto \frac{1}{64\pi^2} \frac{k\alpha}{p_i^2} \sum_{\lambda} \langle \mathbf{k}\lambda | \hat{\rho}_\gamma | \mathbf{k}\lambda \rangle \\ &= (1 - S_x - S_y - S_z) d\sigma(0,0,0) + S_x d\sigma(1,0,0) \\ &+ S_y d\sigma(0,1,0) + S_z d\sigma(0,0,1) = d\sigma(0,0,0)(1 - S_y C_{20}), \end{aligned} \quad (16)$$

where, in order to derive the last line we have used the symmetry relations (3) and the definition (11) of the correlation coefficient C_{20} .

In addition to the analysis of the differential cross section, Eq. (15) may help us also to study how the polarization of bremsstrahlung photons is affected if the incident electron beam is (partially) polarized. Namely, as follows from Eq. (13), the first Stokes parameter of the emitted radiation can be written as

$$P_1 = \frac{\langle \mathbf{k} + 1 | \hat{\rho}_\gamma | \mathbf{k} - 1 \rangle + \langle \mathbf{k} - 1 | \hat{\rho}_\gamma | \mathbf{k} + 1 \rangle}{\sum_{\lambda=\pm 1} \langle \mathbf{k}\lambda | \hat{\rho}_\gamma | \mathbf{k}\lambda \rangle}.$$

By inserting Eq. (15) into this expression we immediately find

$$\begin{aligned} P_1 &= \frac{1}{d\sigma(0,0,0)(1 - S_y C_{20})} \\ &\times [(1 - S_x - S_y - S_z) d\sigma(0,0,0) P_1(0,0,0) \\ &+ S_x \sigma(1,0,0) P_1(1,0,0) + S_y d\sigma(0,1,0) P_1(0,1,0) \\ &+ S_z d\sigma(0,0,1) P_1(0,0,1)] \\ &= \frac{P_1(0,0,0)(1 - S_y) + S_y P_1(0,1,0)(1 - C_{20})}{1 - S_y C_{20}}, \end{aligned} \quad (17)$$

where again the symmetry arguments (3) and (4) were used. In a similar way one derives the formula

$$P_2 = \frac{S_x P_2(1,0,0) + S_z P_2(0,0,1)}{1 - S_y C_{20}} \quad (18)$$

for the second Stokes parameter which, together, with P_1 uniquely defines the linear polarization of the bremsstrahlung radiation.

Equations (16)–(18) define the intensity and polarization of the photons emitted by partially polarized electrons. In the following we show that these equations can be understood rather intuitively. Without loss of generality, we can assume that the electron beam consists of electrons polarized along or opposite to the axes \hat{x} , \hat{y} , and \hat{z} . We also assume that the numbers of these electrons, $N_{\uparrow x}, N_{\downarrow x}, N_{\uparrow y}, N_{\downarrow y}, N_{\uparrow z}$, and $N_{\downarrow z}$, are such that $N_{\uparrow x} > N_{\downarrow x}$, $N_{\uparrow y} > N_{\downarrow y}$, and $N_{\uparrow z} > N_{\downarrow z}$. Such a beam can be represented as three beams in pure polarized states with numbers of electrons $N_{\uparrow x} - N_{\downarrow x}, N_{\uparrow y} - N_{\downarrow y}$, and $N_{\uparrow z} - N_{\downarrow z}$ and an additional beam of unpolarized electrons with the number $2(N_{\downarrow x} + N_{\downarrow y} + N_{\downarrow z})$. The proportions of the electrons in these beams, $S_x = (N_{\uparrow x} - N_{\downarrow x})/N$, $S_y = (N_{\uparrow y} - N_{\downarrow y})/N$,

$S_z = (N_{\uparrow z} - N_{\downarrow z})/N$, and $S_o = 2(N_{\downarrow x} + N_{\downarrow y} + N_{\downarrow z})/N$ are such that $S_o + S_x + S_y + S_z = 1$. Here N is the total number of the electrons.

The light intensity emitted by unpolarized electrons is I° and the light intensities emitted by electrons polarized along the \hat{x} , \hat{y} , and \hat{z} axes are I^x , I^y , and I^z , such that $I^\circ + I^x + I^y + I^z = I$. The total light intensity emitted in a given direction is then

$$\begin{aligned} I &\propto d\sigma(0,0,0)S_o + d\sigma(1,0,0)S_x \\ &\quad + d\sigma(0,1,0)S_y + d\sigma(0,0,1)S_z \\ &= d\sigma(0,0,0)(1 - S_y) + d\sigma(0,1,0)S_y \\ &= d\sigma(0,0,0)(1 - S_y C_{20}). \end{aligned}$$

This equation coincides with (16). The Stokes parameters P_1 and P_2 are by definition

$$\begin{aligned} P_{1,2} &= \frac{\sum_{i=o,x,y,z} (I_{0^\circ,45^\circ}^i - I_{90^\circ,135^\circ}^i)}{I} = \sum_{i=o,x,y,z} P_{1,2}^i \frac{I^i}{I} \\ &= P_{1,2}(0,0,0) \frac{S_o}{1 - S_y C_{20}} + P_{1,2}(1,0,0) \frac{S_x}{1 - S_y C_{20}} \\ &\quad + P_{1,2}(0,1,0) \frac{1 - C_{20}}{1 - S_y C_{20}} S_y + P_{1,2}(0,0,1) \frac{S_z}{1 - S_y C_{20}}. \end{aligned}$$

It is easy to see that these equations are equivalent to (17) and (18).

IV. EXPERIMENTAL TECHNIQUE

We did the measurement at a test stand of a 100 keV source of polarized electrons at Technische Universität Darmstadt, Germany [51]. A GaAsP superlattice strained-layer photocathode produced longitudinally polarized electrons when it was illuminated by circularly polarized laser light of 808 nm wavelength. Circular light polarization was attained by a combination of a linear polarizer and a Pockels cell. The helicity of light was switched from positive to negative by changing the bias polarity of the Pockels cell. This rotated the electron spin by 180° , while preserving all other experimental conditions such as the beam trajectory, degree of polarization, etc. The electrons were accelerated electrostatically to 100 keV and the beam intensity was $0.1 \mu\text{A}$ up to $1 \mu\text{A}$.

The degree of polarization of the electron beam was obtained by the Mott scattering polarimetry technique [52,53]. Since Mott scattering is sensitive to transverse spin components only, the electron spin was rotated from the longitudinal to the transverse direction with the help of a Wien filter [54]. The electrons, elastically scattered in a gold foil, were detected at 120° relative to the beam direction by four silicon surface-barrier detectors mounted at azimuthal angles such that they formed a square with two sides parallel and the other two sides perpendicular to the reaction plane. The electron beam polarization was deduced from the measured left-right asymmetry with respect to the plane defined by the electron momentum and spin. Effects of multiple scatterings were controlled by measurements with targets of different thicknesses (40–500 nm) and an interpolation to zero thickness; see Ref. [51]. The measured degree of electron polarization was $S = 0.75 \pm 0.04$. In order to obtain the maximum degree of

transversely polarized electron beam, we tuned the Wien filter to produce the maximum left-right asymmetry of the electron scattering intensities. The maximum asymmetry is obtained in the case when the electron spin is oriented perpendicular to the scattering plane in the electron rest frame. In contrast to that, in the laboratory frame the transverse electron spin polarization cannot be defined universally, because due to the Lorentz transformations it depends on the observation angle.

Compton and Rayleigh scattering techniques were used to measure the photon linear polarization. The photons scatter predominantly perpendicular to the polarization plane. Their angular distribution carries information on both the degree and the angle of the incoming photon linear polarization. In the case of Compton scattering it is described by the well known Klein-Nishina Compton scattering differential cross section [22],

$$\frac{d\sigma}{d\Omega} \propto \left(\frac{\hbar\omega'}{\hbar\omega}\right)^2 \left(\frac{\hbar\omega'}{\hbar\omega} + \frac{\hbar\omega}{\hbar\omega'} - 2 \sin^2 \xi \cos^2 \varphi\right). \quad (19)$$

Here $\hbar\omega$ and $\hbar\omega'$ are the incoming and scattered photon energies, and the angles are explained in Fig. 2. This polarimetry principle has been used since 1950 [55]. However, our realization of it allows for a simultaneous photon detection at several scattering angles and thus has high efficiency and resolution. In addition, the Rayleigh scattering technique [56] was used.

A high-purity segmented planar germanium detector was used to observe the scattered photons. Its active area of $5 \times 5 \text{ cm}^2$ is segmented into a 5×5 matrix of square pixels. Each pixel is equipped with an individual charge-sensitive preamplifier and a 100 MHz sampling analog-to-digital converter. The sampled detector signals were analyzed using a moving window deconvolution algorithm, yielding for the experimental conditions an energy resolution of 2.7 keV at

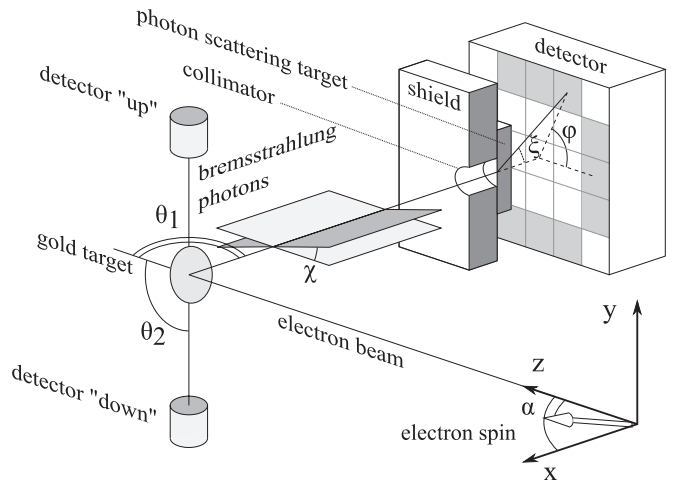


FIG. 2. Scheme of the experimental setup (the shielding and the scattering target are shown in section). The electron spin was oriented within the (x,z) plane at an angle α with respect to \hat{z} . The photons are scattered at the polar angle ξ with respect to their initial direction. The azimuthal photon scattering angle with respect to the reaction plane (x,z) is denoted by φ . Detector segments used in analysis are indicated in gray. The photons emitted in the (y,z) at the angle θ_2 were detected by two detectors denoted “up” and “down.”

60 keV. The thickness of the detector is 2 cm. Its vacuum window is a combination of 0.7 mm aluminum and 2 mm epoxy. It resulted in the detector's absolute efficiency of nearly 100% at 90–100 keV.

Electrons collided with a free-standing gold-foil target of 200 nm thickness ($390 \mu\text{g}/\text{cm}^2$) and produced bremsstrahlung. The detector was placed at a distance of 15 cm from the gold target (see Fig. 2) behind a 3-mm-thick vacuum chamber quartz window (not shown). The window transmission at 90–100 keV was greater than 86%. GEANT4 Monte Carlo simulations [57,58] have shown that the influence of photon scattering in the window on photon linear polarization was negligible. Lead walls with a thickness of 1 cm shielded the detector from unwanted x rays. The bremsstrahlung was collimated by a 1 cm round opening in the shield, which selected photons emitted at an angle of $\theta_1 = 90^\circ \pm 3^\circ$ with respect to the initial electron beam direction. The detector was placed perpendicular to the collimated photon beam and its center was aligned with the photon beam axis. A photon scattering target has been placed behind the collimator at a distance of 2.7 cm in front of the detector's crystal. With this arrangement the outer segments, used in the data analysis, could observe the scattered photons only. The photon scattering angle was $20^\circ < \xi < 48^\circ$. The inner segments were not read out because they were irradiated by unscattered x rays.

Two variations of the Compton polarimetry techniques exist. Both of them measure the azimuthal distributions of the Compton scattering events. In order to unambiguously reconstruct these events, i.e., to separate them from the background and to determine the scattering direction, one technique uses a scatterer which is a detector itself—the “active” scatterer. In this technique the scattered photons and the recoiled electrons are detected in coincidence in different segments of the segmented detector [59,60]. The energies of the scattered photon and the recoiled electron help in filtering the ambient background radiation. Therefore this technique has excellent background filtering capabilities. However, at x-ray energies below 100 keV most of the events are direct photoelectric absorptions of the incoming photons or Compton scatterings and photoabsorptions in the same pixel. This limits the maximum allowed incoming photon flux, because these events are not analyzed, but are still registered by the data acquisition system. Due to these limitations we decided against using this technique.

Instead we used the other variation of the Compton technique. In this technique the scattering target is not a detector; thus the recoiled electrons are not detected. However, the geometry of the setup, i.e., the shielding, collimation, and placement of the segmented detector, selects the scattered events. We selected this approach for its ability to work with high photon rates and its usefulness at an energy of ≈ 100 keV. We used the material and the thickness of the target that are optimum for this energy region. An iron scatterer of 5 mm thickness effectively photoabsorbed photons with energies below ≈ 75 keV and scatter the others. In addition it produced a significant proportion of Rayleigh-scattering events. The outer segments detected the photons scattered at different azimuthal angles, and we extracted the polarization from the observed angular distribution. Since every registered event was the scattering event, the data acquisition system

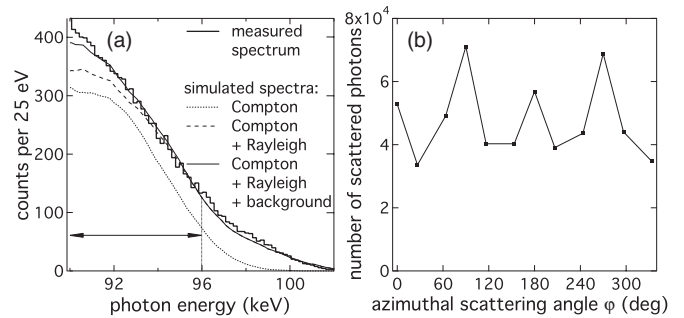


FIG. 3. (a) Measured and simulated spectra. Contributions of Compton and Rayleigh scatterings as well as background are shown separately. The spectral interval used in the analysis is indicated. (b) Integrated number of scattering events in the indicated spectral interval in each detector pixel as a function of the azimuthal scattering angle φ .

was not loaded by the overwhelming majority of direct photoabsorption events. Thus much higher photon flux could be accepted and high-statistics data were collected for each electron spin orientation in only a few hours of beam time.

Two more scintillator detectors were mounted at the setup in order to observe bremsstrahlung photon emission asymmetry by transversely polarized electrons. The details of this part of the setup are discussed in Sec. VD.

V. DATA ANALYSIS

The high-energy part of the photon spectrum is shown in Fig. 3(a). Due to Compton scattering in iron and the imperfect energy resolution of the detector, the bremsstrahlung spectrum has no sharp cutoff at the energy of 100 keV. However, note that this is not an indication of “thick target” bremsstrahlung [61]; the cutoff was present in the spectrum of the inner segments before the Compton scattering target was installed. With a total event rate of ≈ 3000 counts per second, ambient background events constituted less than 1% of the spectrum, and no pileup was seen. The contributions of Compton and Rayleigh scatterings have been determined via Monte Carlo simulations using the GEANT4 toolkit. Compton scattering accounts for 78% of events in the indicated interval.

Note that due to the electron recoil in Compton scattering

$$\hbar\omega' = \frac{\hbar\omega}{1 + \frac{\hbar\omega}{mc^2}(1 - \cos\xi)}, \quad (20)$$

the Compton part of the measured spectrum is shifted to lower energies. The elastic Rayleigh scattering is therefore dominant at energies higher than 96 keV. The analysis of this part of the spectrum also yields polarization information. The application of the Rayleigh polarimetry technique for bremsstrahlung is presented in [22] and will not be discussed further in this article.

The radiation background originated from the bremsstrahlung of the electrons which elastically scattered in the gold target and hit the chamber quartz window. Except for this window the chamber was covered by lead. Monte Carlo simulations have shown that 3% of all electrons hit the window. We adopted the following model to calculate the emitted background radiation. Electrons

lose energy as they penetrate through quartz. Their energy was calculated as a function of the penetration depth using the continuous-slowning-down approximation [62]. For each electron energy the penetration depth provided an effective thickness of the quartz layer as a bremsstrahlung target. And for each such layer the bremsstrahlung spectrum was calculated and summed up. The background spectrum is shown in Fig. 3(a). Its contribution to the selected spectral interval was 7%. At lower energies its contribution was larger. Therefore we restricted our further analysis to photon energies higher than 90 keV.

The total number of scattered photons I in the selected interval was counted; see Fig. 3(b) for each segment of the detector. In each segment the scattered photons were observed at a different azimuthal angle φ . The photon polarization was extracted from the scattered photon angular distributions $I(\varphi)$. The intensity distribution depends on polarization [see Eq. (19)] as well as on the scattering geometry and the solid angles of the individual segments. The latter two effects can be canceled by an intensity normalization $J(\varphi) = \frac{I(\varphi+90^\circ)+I(\varphi+270^\circ)}{I(\varphi)+I(\varphi+180^\circ)}$, which uses the detector's fourfold rotational symmetry; see Fig. 4(a). The same normalization minimizes the effects of a possible slight off-axis misalignment of the collimator.

As a result of the Compton and Rayleigh scattering cross sections the scattered photon azimuthal angular distribution was $F(\psi, M) = \frac{1-M \cos^2(\psi+90^\circ)}{1-M \cos^2(\psi)}$. Here ψ is the azimuthal angle of photon scattering with respect to the photon polarization plane, and M is a modulation amplitude. It depends on the degree of polarization and the polar angle ξ between the initial and scattered photon directions [56,59]: $M = 2 \sin^2 \xi / (\frac{\hbar\omega'}{\hbar\omega} + \frac{\hbar\omega}{\hbar\omega'})$; see Eq. (19). Here $\hbar\omega'$ depends also on ξ ; see Eq. (20). The photon linear polarization was azimuthally tilted by an angle χ with respect to the reaction plane. In addition the detector was also tilted by an angle $\varphi_0 = -2.81^\circ$ with respect to the same plane. The azimuthal angular distribution of the scattered photons is therefore $F(\varphi + \varphi_0 + \chi, M)$. By fitting this function to $J(\varphi)$ the tilt angle χ can be extracted. However, more accurate results are obtained by adopting a procedure described in the next section.

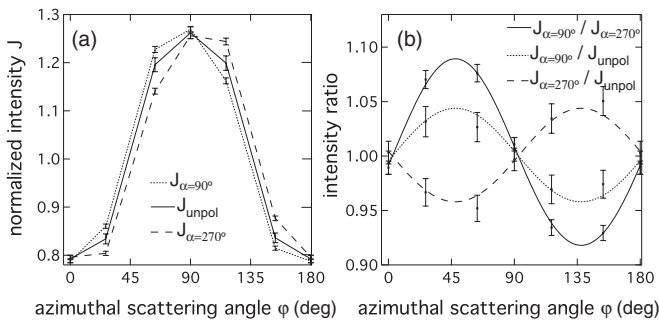


FIG. 4. (a) Angular distribution of the normalized scattering intensity for scattering of bremsstrahlung from the spectral interval a from the electrons spin polarized collinearly [$J_{\alpha=90^\circ}(\varphi)$] and anticollinearly [$J_{\alpha=270^\circ}(\varphi)$] to the x axis and unpolarized. The errors are statistical. (b) Intensity ratio $J_{\alpha=90^\circ}(\varphi)/J_{\alpha=270^\circ}(\varphi)$.

A. Polarization correlation $P_2(1,0,0)$

The polarization correlation $P_2(1,0,0) = -C_{11}$ describes the change of the second Stokes photon polarization parameter P_2 as a function of the transverse electron spin component within the reaction plane. Since $P_1(1,0,0) = P_1(-1,0,0)$, the total degree of photon linear polarization is the same for oppositely oriented spins of the electron beam, i.e., for the spin orientations collinear ($\alpha = 90^\circ$) and anticollinear ($\alpha = 270^\circ$) to \hat{x} . However, the angles of polarization are different by 2χ .

The angular shift 2χ between the measured normalized distributions $J_{\alpha=90^\circ}(\varphi)$ and $J_{\alpha=270^\circ}(\varphi)$ is related to the Stokes parameters by $\tan 2\chi = P_2/P_1$. These angular distributions are shifted by the angle χ to the opposite sides of the reaction plane and their modulations are the same. Therefore, the averaged distribution $[J_{\alpha=90^\circ}(\varphi) + J_{\alpha=270^\circ}(\varphi)]/2$ must be centered with respect to the reaction plane. The value of $M = 25\%$ was obtained by fitting of $F(\varphi + \varphi_0, M)$ to this distribution.

To cancel the effects of geometric differences of individual segments, the scattering angular distributions were normalized, $\frac{J_{\alpha=90^\circ}(\varphi)}{J_{\alpha=270^\circ}(\varphi)}$; see Fig. 4(b). The modulation of the normalized distribution is a result of nonzero χ , i.e., it is zero for $\chi = 0$. To extract χ , the normalized distribution has been fitted with a function $\frac{F(\varphi+\varphi_0+\chi, M)}{F(\varphi+\varphi_0-\chi, M)}$, treating χ as a single free parameter. From this fit the value $\frac{C_{11}}{C_{03}} = -\frac{P_2(1,0,0)}{P_1(0,0,0)} = -\frac{P_2(S,0,0)}{SP_1(0,0,0)} = -\frac{\tan 2\chi}{S}$ is obtained. The results are shown in Table II. Average initial photon energies were obtained via Monte Carlo simulations.

B. Thick target effects

Multiple electron scattering in the gold target distributes the individual electron directions. If one assumes a pure Rutherford scattering, this distribution is axially symmetric with respect to the initial electron momentum direction. The individual bremsstrahlung reaction planes, defined by the electron and the photon momenta, are also distributed. Since the individual photons are linearly polarized relative to their reaction planes, the average degree of photon polarization is reduced. However, due to the axial symmetry of the multiple scattering the average electron direction before photon emission coincides with the direction of the electron before it entered the target. Because of this the average reaction plane is unaffected by the multiple scattering. Therefore the angle of photon polarization is also unaffected.

In addition to that, Mott scattering causes a deflection of the average electron beam direction perpendicular to the reaction plane. This deflection depends on the sign and the degree of

TABLE II. Polarization correlations measured at the hard-end interval 95.5 ± 2.4 keV of the photon spectrum observed at $\theta = 90^\circ \pm 3^\circ$. The 100 keV electrons collided with a gold ($Z = 79$) target. The theoretical predictions for the exact hard end of the spectrum are shown for comparison. The error intervals $\pm\sigma$ correspond to two standard deviations. The photon polarization tilt angle χ_0 is given for 100% polarized electrons.

Polarization correlation	Experiment	Theory
$\frac{C_{11}}{C_{03}} = -\frac{P_2(1,0,0)}{P_1(0,0,0)} = -\tan 2\chi_0$	-0.23 ± 0.03	-0.229
$\frac{C_{31}}{C_{03}} = \frac{P_2(0,0,1)}{P_1(0,0,0)} = \tan 2\chi_0$	0.073 ± 0.014	0.069

electron polarization. It also depends on the thickness of the target and should vanish with infinitely thin targets. Due to the net beam deflection the polarization plane is tilted with respect to the reaction plane. This tilt, however, is not related to the tilt caused by the bremsstrahlung polarization correlation $P_2(1,0,0)$. These two distinct effects can be deconvoluted in a series of measurements with gold targets of different thicknesses. However, Monte Carlo simulations show that the thickness of the target used in the present experiment leads to a negligible Mott scattering effect [63]. Hence, only one measurement was carried out.

C. Polarization correlation $P_2(0,0,1)$

The polarization correlation $P_2(0,0,1) = C_{31}$ describes the change of the second Stokes photon polarization parameter P_2 as a function of the longitudinal electron spin component. Similarly to the previous case, $P_1(0,0,1) = P_1(0,0,-1)$ holds, and the total degree of photon linear polarization is the same for oppositely oriented spins of the electron beam, i.e., for electron beams polarized collinearly ($\alpha = 0^\circ$) and anticollinearly ($\alpha = 180^\circ$) with respect to their momentum direction. The angular shift 2χ between the measured distributions $J_{\alpha=0^\circ}(\varphi)$ and $J_{\alpha=180^\circ}(\varphi)$ is related to $P_2(0,0,1)$ by $\tan 2\chi = P_2/P_1$. The details of the analysis are identical to the case of the polarization correlation $P_2(1,0,0)$. They are also described in [22]. From this measurement the value $\frac{C_{31}}{C_{03}} = \frac{P_2(0,0,1)}{P_1(0,0,0)} = \frac{P_2(0,0,S)}{SP_1(0,0,0)} = \frac{\tan 2\chi}{S}$ is obtained.

The tilt angle χ was measured with a precision of $\sigma = 0.3^\circ$. This is a significant achievement of Compton polarimetry. The uncertainty is dominated by statistics. Such precision is achieved in only a few hours of beam time and holds the promise of further improvements with longer measurements.

D. Photon emission asymmetry from transversely polarized electrons

The asymmetry of bremsstrahlung photon emission with respect to the plane defined by the electron momentum and the electron spin, $C_{20} = -\frac{d\sigma(0,1,0) - d\sigma(0,-1,0)}{d\sigma(0,1,0) + d\sigma(0,-1,0)}$, is a well-known phenomenon. Within this experiment it was observed and applied for electron beam polarimetry. For reasons described below, the results obtained—or the values deduced for the correlation C_{20} —are not competitive with those of earlier published works [31–35].

Two scintillating photon detectors were used to measure the bremsstrahlung spectra. They were placed in the (y,z) plane at the angle $\theta_2 \approx 120^\circ$. A $\text{LaCl}_3(\text{Ce})$ scintillator was mounted above the (x,z) plane (designated “up”) and a $\text{LaBr}_3(\text{Ce})$ scintillator was mounted below it (designated “down”). Copper plates of 5 mm thickness were mounted in front of the scintillators in order to reduce the count rate at low photon energies. The scintillators were equipped with photomultiplier tubes, preamplifiers, and 100 MHz sampling analog-to-digital converters. The energy resolutions of both scintillators were identical: 15 keV when measured at 60 keV. The spectra observed with these detectors are shown in Fig. 5(a). The spectral interval used for the intensity measurement is indicated.

The light output of the scintillators quickly drifted in time due to temperature variations. The closed experimental

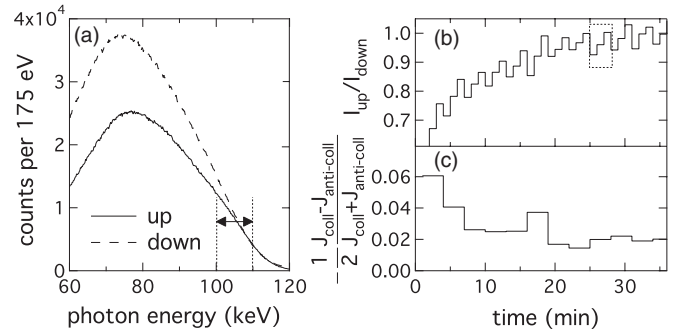


FIG. 5. (a) Spectra observed by the $\text{LaCl}_3(\text{Ce})$ (up) and the $\text{LaBr}_3(\text{Ce})$ (down) scintillators. The corresponding integrated intensities in the marked energy interval are I_{up} and I_{down} . (b) The intensity ratio $J = I_{\text{up}}/I_{\text{down}}$ as a function of time. The electron beam polarization was changed every minute repeatedly as $[(S_x, 0, 0) \Rightarrow (0, 0, 0) \Rightarrow (-S_x, 0, 0)]$; an example cycle is marked. (c) The normalized intensity ratio $\frac{1}{2}(J_{\text{coll}} - J_{\text{anticoll}})/(J_{\text{coll}} + J_{\text{anticoll}})$ as a function of time.

room heated up by several degrees during measurements and quickly cooled during frequent interruptions. This resulted in drifts of the x-ray energies measured by the scintillators, which induced a variation of the intensity in the selected spectral interval. In order to minimize this effect, the following measurement technique was adopted. Three measurements of photon intensities I_{up} and I_{down} were performed with the electron beam polarized as $(S_x, 0, 0)$, $(0, 0, 0)$, and $(-S_x, 0, 0)$. Each measurement took 1 min, and this cycle was repeated several times. The ratio of the photon intensities in these cycles, $J = I_{\text{up}}/I_{\text{down}}$, is shown in Fig. 5(b). The average ratio in each of these cycles was used for normalization. The average modulation is

$$\frac{1}{2} \left\langle \frac{J_{\text{coll}} - J_{\text{anticoll}}}{J_{\text{coll}} + J_{\text{anticoll}}} \right\rangle \approx \frac{d\sigma(S_x, S_y, S_z) - d\sigma(-S_x, S_y, S_z)}{d\sigma(S_x, S_y, S_z) + d\sigma(-S_x, S_y, S_z)} = -C_{20} S_x; \quad (21)$$

see Fig. 5(c). This is an approximate expression for small C_{20} .

The value obtained for $C_{20} = 0.035 \pm 0.010$ is significantly smaller than the predicted value $C_{20}^{\text{theor}} \approx 0.10$. This disagreement originates from the lack of shielding of the scintillators against unwanted ambient x rays. Most of this x-ray ambient background, scattered across the experimental room, was produced in the electron beam dump located 50 cm downstream of the gold target. It contributed to the scintillators’ spectra and thus reduced the electron-spin-dependent intensity modulation. However, despite this, the observed modulation is proportional to S_x and thus can be used for electron beam polarimetry.

The germanium segmented detector response was free from the temperature-dependent drifts and it was well shielded from the unwanted ambient x rays. Thus accurate measurements of C_{20} should in the future be done with shielded semiconductor detectors or temperature-stabilized scintillating detectors.

VI. CLASSICAL INTERPRETATION

A. Polarization correlations $P_2(1,0,0)$ and $P_2(0,0,1)$

The observed rotation of photon linear polarization can be understood in terms of classical physics. It indicates a

spin-induced dynamics of the relativistic electron in scattering from a Coulomb potential [22]. The classical approximation for Coulomb scattering is valid for energies $T \lesssim 20Z^2$ eV [64]. At higher energies quantum-mechanical effects become important. This happens when the distance of the closest approach is less than half the de Broglie wavelength $\lambda = 2\pi\hbar/p$ for electron scattering through an angle of 90° . For gold ($Z = 79$) this yields $T \lesssim 125$ keV. However, the classical results may be qualitatively valid up to even higher energies of MeV [65].

In the following we will present a classical explanation for the electron spin effects on the emitted bremsstrahlung. A spinless particle in a central Coulomb potential moves on a trajectory contained within a single plane defined by the particle's conserved angular momentum $\mathbf{L} = \mathbf{r} \times \boldsymbol{\beta}$. At low energies the spin-induced forces are small and they do not deflect the trajectory out of this plane. At relativistic energies, on the other hand, they contribute to the dynamics considerably. In the electron rest frame the moving nucleus induces a magnetic field \mathbf{H} perpendicular to the scattering plane. The electron spin precesses in this field [66]. This precession is one of the aspects of the spin-orbit interaction. By making the approximation of a uniform magnetic field, we apply the Thomas–Bargmann–Michel–Telegdi equation [66,67] for the torque on the spin:

$$\dot{\mathbf{S}} = \mathbf{S} \times [\mathbf{E} \times \boldsymbol{\beta}] \frac{e}{mc} \left(g - 2 + \frac{1}{\gamma + 1} \right). \quad (22)$$

Here $\boldsymbol{\beta}$ is the electron velocity, $g = 2.00116$ is the electron gyromagnetic ratio, and \mathbf{E} is the Coulomb field of the nucleus; see Fig. 6. Since the total angular momentum must be conserved, the orbital momentum also precesses: $\dot{\mathbf{S}} = -\dot{\mathbf{L}}$. As a result the electron moves out of the initial scattering plane and its trajectory from being two dimensional becomes three dimensional.¹

The spin precession is defined by the electric field of the nucleus. The same field deflects the electron. The net spin precession thus depends on the electron scattering angle. We describe the electron scattering by the Lorentz force:

$$\dot{\boldsymbol{\beta}} = \boldsymbol{\beta} \times [\mathbf{E} \times \boldsymbol{\beta}] \frac{e}{mc} \frac{\gamma}{\gamma^2 - 1}. \quad (23)$$

Equations (22) and (23) can be rewritten as $\dot{\mathbf{S}} = \mathbf{S} \times \boldsymbol{\Omega}_S$ and $\dot{\boldsymbol{\beta}} = \boldsymbol{\beta} \times \boldsymbol{\Omega}_\beta$, where $\boldsymbol{\Omega}_S$ and $\boldsymbol{\Omega}_\beta$ are the angular velocities of the electron spin and the electron momentum vectors, which are related to each other by

$$\boldsymbol{\Omega}_S = [(g - 2)(\gamma + 1) + 1] \left(1 - \frac{1}{\gamma} \right) \boldsymbol{\Omega}_\beta. \quad (24)$$

For the electron energy of 100 keV Eq. (24) yields $\boldsymbol{\Omega}_S = 0.16\boldsymbol{\Omega}_\beta$, and for an electron scattering angle of 90° the angle of the spin rotation is 15° . For our energy and geometry $\mathbf{S} \approx \mathbf{L}$. Therefore the orbital momentum \mathbf{L} and the scattering plane rotate also by 15° .

¹The exact analytical solution for the electron trajectory in the nonrelativistic case is presented in [68]. The relativistic case is described in [69].

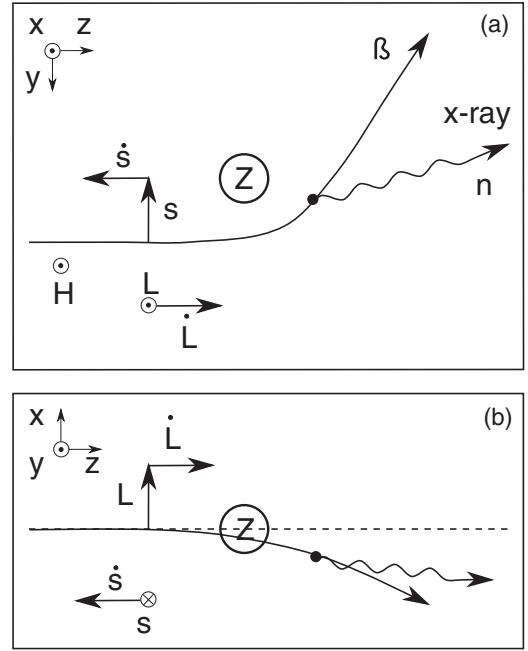


FIG. 6. (a), (b) Classical description of radiation emitted in Coulomb scattering. The direction of the emitted photon is given by a unit vector \mathbf{n} ; the electron velocity is $\boldsymbol{\beta} \cdot c$; the spin of the electron is denoted by \mathbf{S} and the electron angular momentum by \mathbf{L} . The spin precesses in the magnetic field \mathbf{H} motionally induced by the nucleus in the electron rest frame. (b) It induces the precession of the angular momentum \mathbf{L} , which rotates the plane of the electron motion. The dashed line indicates the initial scattering plane.

The direction of the electron acceleration $\dot{\boldsymbol{\beta}}$ lies within the scattering plane and defines the polarization of the radiated wave [70]:

$$\mathbf{E}(\mathbf{r}, t) = \frac{e}{c} \frac{\mathbf{n} \times \{(\mathbf{n} - \boldsymbol{\beta}) \times \dot{\boldsymbol{\beta}}\}}{(\mathbf{n} - \boldsymbol{\beta})^3 r} \Big|_{\text{ret}}, \quad (25)$$

where \mathbf{n} is a unit vector in the direction of the emitted photon. Since the instantaneous scattering plane turns out of the initial scattering plane the photon polarization turns together with it.

In this experiment we were interested in how the scattering plane is oriented at the moment of photon emission. The scattering plane is defined by two vectors—by the electron direction at this moment and its acceleration direction. The first vector coincides with the averaged photon emission direction. The photons are peaked in the electron direction due to the relativistic Lorentz angle transformation. This can be seen in Eq. (25). The second vector, the electron acceleration, coincides with the photon polarization vector, as also seen in Eq. (25).

We observe that the scattering plane, defined in this way, does not contain the initial electron direction. This is a direct indication of the rotation of the scattering plane, or rotation of the orbital momentum \mathbf{L} . According to the above arguments, the angle of rotation is fully determined by just the direction of the emitted photon and the incoming electron energy; see Eq. (24). It does not depend on the photon energy. One of the recent measurements confirms this [23].

In our arguments we assumed peaking of the photon emission along the electron direction just before the photon

emission. The perfect alignment of these directions occurs only in an ultrarelativistic situation. For the semirelativistic regime of 100 keV we should consider the distribution of the emitted photons with respect to the electron direction $\frac{dP}{d\Omega}(\theta, \phi)$ (the Poynting vector), where θ is the angle between $\boldsymbol{\beta}$ and \mathbf{n} [70] and ϕ is the azimuthal angle. The averaged projection of the emitted photon direction on the electron direction before the photon emission $\overline{\boldsymbol{\beta} \cdot \mathbf{n}}/\beta$ describes how well the geometry is defined for a given electron energy (here $\boldsymbol{\beta}/\beta$ is a unit vector in the direction of the electron momentum):

$$\frac{\overline{\boldsymbol{\beta} \cdot \mathbf{n}}}{\beta} = \frac{\int \cos \theta \frac{dP}{d\Omega} d\Omega}{\int \frac{dP}{d\Omega} d\Omega} = \beta. \quad (26)$$

Here we used an approximation of $\boldsymbol{\beta} \perp \dot{\boldsymbol{\beta}}$ to simplify the analytical expression for the Poynting vector [70]. The geometry is perfectly defined in the relativistic case $\beta \rightarrow 1$ and completely undefined in the nonrelativistic $\beta \rightarrow 0$. In particular it indicates that no rotation of linear polarization is expected for nonrelativistic electrons. For 100 keV this yields $\overline{\boldsymbol{\beta} \cdot \mathbf{n}}/\beta = \beta = 0.55$ and thus the net polarization rotation angle is reduced to 8° .

This simplified classical model thus predicts the order of magnitude of the rotation angle of linear polarization. The experimental angle for the fully transversely polarized electron beam is 6.5° . In this case, for the photon emission at 90° , $\dot{\mathbf{L}}$ is perpendicular to \mathbf{n} (see Fig. 6), and the rotation of the scattering plane directly corresponds to the rotation of the photon polarization plane. For longitudinally polarized electrons, on the other hand, $\dot{\mathbf{L}}$ is along \mathbf{n} and thus the rotation of the scattering plane has a much smaller effect on the rotation of the photon polarization. This explains why we observed a smaller angle of photon polarization of 2.1° in this case.

With the help of this model we conclude that in this experiment we have observed that the electron scattering trajectory is not confined to a single scattering plane. Such an observation is not possible in a typical scattering experiment, since the observable macroscopic electron directions before and after the collision always lie in one plane. In contrast to those experiments we probed the orientation of the scattering plane *during* the collision by using the bremsstrahlung photons' linear polarization. This model also explains why a nonzero electron spin component perpendicular to the reaction plane appears in the case of scattering (without photon emission) of electrons initially polarized within the scattering plane, as was observed in earlier experiments [71].

B. Polarization correlation $d\sigma(\mathbf{0}, \mathbf{1}, \mathbf{0})$

When the electron spin is oriented perpendicular to the scattering plane the spin-induced force is different from the one described in the previous sections. This force is confined to the electron scattering plane. Therefore, this plane contains the whole electron trajectory. No spin precession is involved. On the other hand the nonuniformity of the Coulomb field plays a major role.

The left-right asymmetry of Mott scattering with respect to the plane defined by the electron spin and the momentum directions is well understood [24,25]. The magnetic field \mathbf{H} , induced by the nucleus moving in the rest frame of the electron,

produces an extra component to the scattering potential, $-\boldsymbol{\mu}\mathbf{H}$. The sign of this component is different for the electrons scattering to the left and to the right, thus producing the scattering asymmetry.

The spin-induced force is the result of the nonuniformity of this potential, $-\boldsymbol{\mu}\frac{d\mathbf{H}}{dx}$. This force is the same as in the Stern-Gerlach experiment with a nonuniform magnetic field. It was known that it can separate neutral particles into two beams by their spin orientation but cannot do so for charged particles. In the latter case the spin-induced force is much smaller than the Lorentz force. On the other hand, in the case of scattering on the Coulomb potential, the nonuniformity of the field is large, which produces a strong spin asymmetry in Coulomb scattering. And due to the strong angular correlation between the scattered electron and the emitted photon, the latter is also asymmetric with respect to the spin plane.

VII. FULLY RELATIVISTIC CALCULATIONS

In addition to the experimental results, Table II also displays the theoretical prediction for the tilt angle χ obtained for the photon high-energy limit where the incident electron transfers all its kinetic energy to the photon, i.e., where $\hbar\omega = T_{\text{kin}} = 100$ keV. To evaluate χ for this particular energy we have extrapolated the results of the radiative recombination (RR) polarization calculations towards the continuum threshold. Such an approach for computing the polarization properties of bremsstrahlung radiation from corresponding RR data has been justified for the tip (threshold) region in a number of works (see, for example, Ref. [43], and references therein). In the present contribution, the polarization of the RR photons emitted due to the capture of longitudinally polarized electrons into bound (high- n) states has been calculated within the fully relativistic theory. Since this theory has been applied very frequently in studying various RR properties, we will not discuss it here and instead refer the reader to Refs. [72–75]. As seen from Table II, the theoretical value of the tilt angle χ , obtained from the extrapolation of the rigorous RR calculations to the tip region, is in good agreement with the experimental findings.

VIII. ELECTRON BEAM POLARIMETRY

We have shown that bremsstrahlung is sensitive to longitudinal as well as transverse electron spin components. We now apply it to electron beam polarimetry. The minimal detector setup consists of a photon linear polarimeter mounted within the (x,z) plane and two conventional photon detectors mounted within the (y,z) plane (the axis \hat{z} is the beam direction), just like the setup of our experiment (see Fig. 2). With this setup all three components of the electron beam polarization can be determined.² The degree of photon linear polarization can potentially give access to the \hat{y} component of the electron beam polarization. This effect, however, up to now has not been observed experimentally. On the other hand, the same \hat{y}

²We note that one can also measure longitudinal as well as transverse electron spin polarizations by means of circular polarimetry of bremsstrahlung [46,76,77]. This technique, however, is beyond the scope of this paper.

component can be measured by two additional conventional photon detectors, mounted within the (x,z) plane, via the left-right asymmetry of the photon emission.

This polarimetry method has the following properties. Electron polarization is completely determined by bremsstrahlung radiation; thus it requires a minimum vacuum setup consisting of only a foil target and a few x-ray windows. It works with intense electron beams (μA), typically used at accelerators. In contrast to that the Mott scattering technique works with strongly reduced currents (nA). It should work efficiently in the energy range of 100 keV up to a few 10 MeV.

A. Theoretical predictions

The optimum conditions for the measurement are realized at the hard-photon end of the spectrum. There the polarization correlations typically reach their maxima [47–49]. This region makes the photon detection free from a Compton-induced background. Compton scattering inside the detector produces a low-energy tail in the measured spectrum. This tail is indistinguishable from the true bremsstrahlung continuum. In order to suppress it, an active anti-Compton shielding or γ -ray tracking [78,79] can be employed. However these methods are technically complicated. On the other hand the very end of the spectrum is always free from this background.

Theoretical predictions for the double-differential cross section $(k/Z^2)d^2\sigma/(dkd\Omega_k)$ and the Stokes parameters P_1 and P_2 at the hard-photon limit for gold are shown in Fig. 7. The differential cross sections favor observations at forward angles. The maximum of the left-right asymmetry of photon emission from transversely polarized electrons $d\sigma(0,0,0) - d\sigma(0,1,0) = d\sigma(0,0,0)C_{20}$ is also shifted to forward angles θ_2 . This asymmetry is used to measure the S_x with a pair of conventional detectors arranged in the (y,z) plane; see Eq. (16). Similarly, with two additional detectors in the (x,z) plane one can measure the S_y component.

The photon linear polarimeter determines the Stokes parameters P_1 and P_2 . The Stokes parameter P_1 is sensitive only to S_y ; see Eq. (17). The Stokes parameter P_2 is sensitive to S_x , S_z , and S_y ; see Eq. (18). But since S_x and S_y are already determined, S_z can be deconvoluted. Thus all three spin components are measured independently.

The sensitivity to the electron spin is highest at one particular photon emission angle θ_0 ($0^\circ < \theta_0 < 180^\circ$) where $P_1(0,0,0)(\theta_0) = 0$. For energies higher than a few hundred keV such an angle always exists. At this angle unpolarized electrons emit unpolarized photons. Polarized photons immediately indicate polarized electrons. The electron polarization changes the degree of photon linear polarization typically by several percent up to several tens of percent; see Fig. 7. Such strong correlations allow all three components of the electron spin to be determined with a precision of a few percent within hours of beam time.

B. Proof-of-principle measurement

For the measurement we used the same setup and the same data analysis technique as described in the previous sections. We limited ourselves to the situation when the electrons are polarized within the reaction plane. The most general situation of arbitrary polarization we leave for the future.

Figure 8 shows the measured photon polarization angle χ as a function of the degree of electron beam polarization for the cases of transverse and longitudinal orientations of electron spin. The values for the solid circles are calculated by comparing the scattering intensity distributions for the photons produced by polarized and unpolarized electron beams, $J_{\alpha=90^\circ}/J_{\text{unpol}}$ and $J_{\alpha=270^\circ}/J_{\text{unpol}}$; compare Figs. 4(a) and 4(b). They lie on a straight line which for mirror symmetry reasons crosses the origin of the coordinates. However, the slope of this line can be determined more accurately from the ratio $J_{\alpha=90^\circ}/J_{\alpha=270^\circ}$; see the solid and the open squares in Fig. 8.

With knowledge of the electron spin orientation (the two angles of the electron spin in the polar coordinates), the degree of electron beam polarization can be determined with the help of theoretical values for C_{31} and C_{11} . For longitudinally polarized electrons the degree of beam polarization is extracted as $S = 0.72 \pm 0.14$ and for transversely polarized electrons as $S = 0.75 \pm 0.09$. The error intervals correspond to 2σ . These values agree well with the value obtained with the Mott technique, $S = 0.75 \pm 0.04$.

The accuracy can be increased significantly with the same level of statistics by measuring the photon polarization at $\theta \approx 140^\circ$ where C_{11} is larger. Moreover, it will further increase (together with the polarization correlations C_{11} and C_{31}) at higher electron energies. Nevertheless, in order to measure the degree of electron beam polarization without knowledge of the spin orientation, the technique should include a simultaneous measurement of the photon emission asymmetry C_{20} .

In order to demonstrate these principles, the electron spins were oriented within the (x,z) plane ($S_y = 0$) at an angle α with respect to the electron beam direction. This angle was set by a Wien filter. Figure 9(a) shows the experimental values for the angle of photon linear polarization, $\chi(\alpha)$. The solid curve is a theoretical prediction for $\chi(\alpha)$:

$$\chi(\alpha) = \frac{1}{2} \arctan \left[S \left(\frac{P_2(001)}{P_1(000)} \cos \alpha + \frac{P_2(100)}{P_1(000)} \sin \alpha \right) \right],$$

where S is the degree of electron beam polarization. Figure 9(b) shows the experimental values of the photon emission asymmetry $k(\alpha) = (J_{\text{pol}} - J_{\text{unpol}})/(J_{\text{pol}} + J_{\text{unpol}})$, where $J = I_{\text{up}}/I_{\text{down}}$. The solid curve is the function

$$K(\alpha) = C_{20}^* S \sin \alpha,$$

where C_{20}^* is the polarization correlation parameter measured in this experiment; see Sec. VD. These two experimental plots are combined in Fig. 10 as values of χ versus K . The ellipse represents the theoretical function $\chi(\alpha)$ plotted versus $K(\alpha)$. It is formed when the total degree of electron polarization S is preserved while the angle of electron polarization α is varied. Each dot on this ellipse corresponds to a specific value of α . For a single measurement of χ and k the values of S_x and S_z can therefore be deconvoluted.

In a general case when the electron spin S is not confined to the (x,z) plane the degree of the electron polarization will change as a function of S_y due to the nonzero correlation parameter $C_{23} = P_1(0,0,0) - P_1(0,1,0)$. The measurement of the degree of electron polarization should lead to the determination of P_1 and therefore to the determination of S_y .

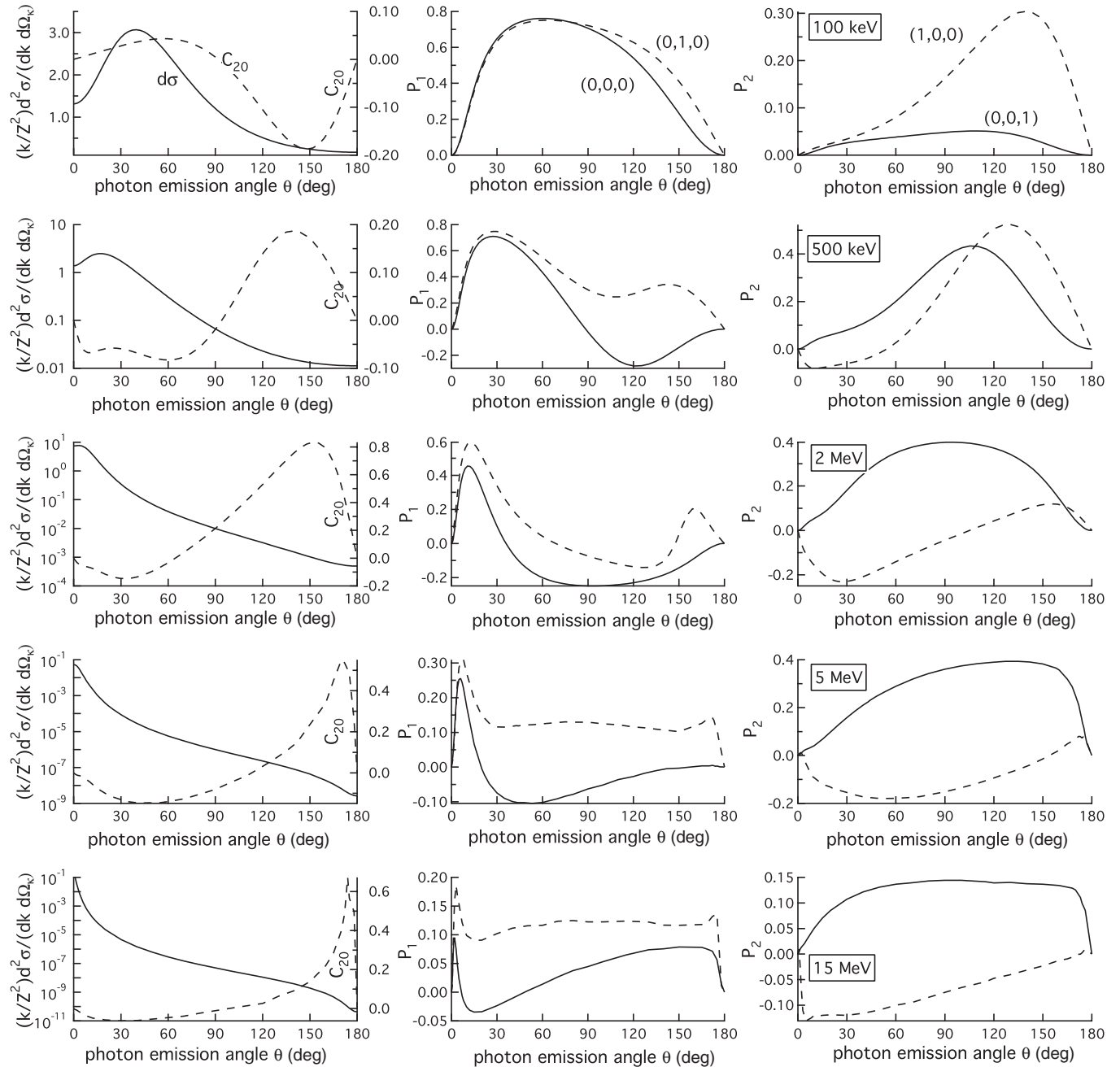


FIG. 7. Theoretical predictions for bremsstrahlung at the hard-photon end of the spectrum for the double-differential cross section $(k/Z^2)d^2\sigma/(dk d\Omega_k)$ and the Stokes parameters P_1 and P_2 and polarization correlation C_{20} . The calculations for the electron beam energies 100 keV, 500 keV, and 2 MeV are performed fully relativistically [48], and the results for 5 and 15 MeV are obtained within the Sommerfeld-Maue approximation [47,49].

All three components of the electron spin can therefore be independently determined.

However, the polarization correlation C_{23} has not been measured so far. Alternatively, one can determine S_y by measuring the photon emission asymmetry with two (nonsegmented) detectors arranged within the (x,z) plane. The alternative setup to determine all three electron spin components would consist of four nonsegmented detectors arranged at the azimuthal angles 0° , 45° , 90° , and 135° and the polar angle θ such that

the product $C_{20}(-\frac{d\sigma}{dkd\Omega_k})^2$ is maximized. These detectors would measure S_x and S_y . Together with these detectors the photon polarimeter would measure S_z .

The efficiency of this polarimetry technique is significantly lower than that of the Mott scattering technique. Mott polarimeters operating with solid targets usually require electron beam currents of the order of nA, whereas for the bremsstrahlung polarimeter a current of at least $1 \mu\text{A}$ would be needed. This will limit the possible applications.

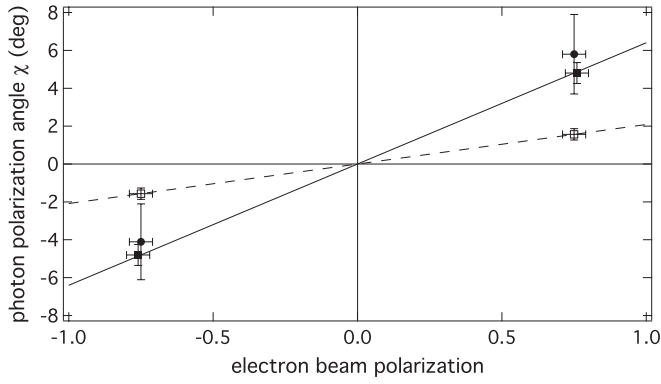


FIG. 8. The photon polarization angle χ as a function of the degree of transverse electron beam polarization (solid symbols, solid line) and longitudinal electron beam polarization (open symbols, dashed line). The error intervals correspond to two standard deviations.

IX. CONSEQUENCES FOR OTHER PHYSICS AREAS

A. Photoelectric effect

Since the physics phenomena of radiative recombination, the photoeffect, and bremsstrahlung at the hard-photon limit are closely related to one another, the present measurement of the bremsstrahlung polarization correlations contributes to the studies of the photoelectric effect and radiative recombination.

Bremsstrahlung at the hard-photon limit is a time reversal of the photoeffect [41–43]. Thus our results with longitudinally polarized electrons can be considered as an observation of a so far experimentally unknown phenomenon—production of longitudinally polarized electrons by photoionization of unpolarized atoms with linearly polarized photons. In the terminology of Pratt *et al.* this is described by the correlation parameter C_{23} [80].

Similarly, the results with transverse polarized electrons indicate a previously experimentally unknown production of transversely polarized electrons by linearly polarized photons. However, this correlation is between the electrons polarized in the reaction plane and photons polarized at 45° to the reaction plane [80]. Pratt *et al.* described it by the correlation parameter C_{21} .

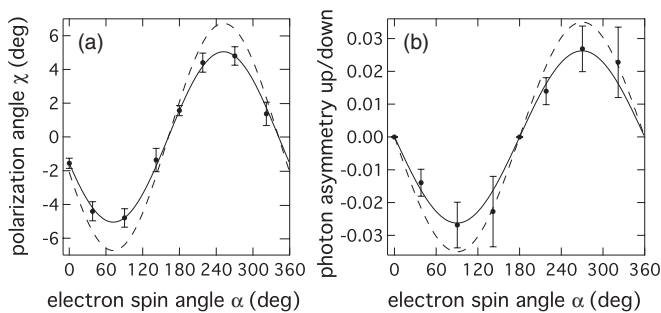


FIG. 9. The photon polarization angle χ (a) and the photon up-down emission asymmetry K (b) as functions of electron spin orientation angle α for electrons polarized within the reaction plane ($S_y = 0$). The solid curves are the predictions for 75% polarized electrons. The dashed curves are the predictions for 100% polarized electrons. The error intervals correspond to two standard deviations.

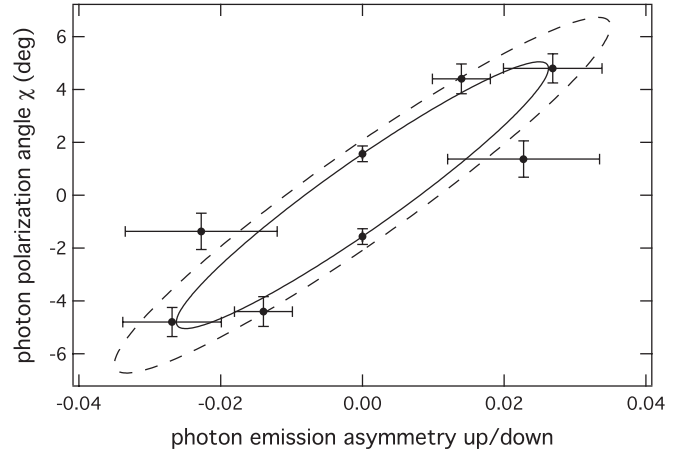


FIG. 10. The photon polarization angle χ as a function of the photon emission asymmetry K for electrons polarized within the reaction plane ($S_y = 0$). The solid curve is the prediction for 75% polarized electrons. The dashed curve is the prediction for 100% polarized electrons.

B. Polarimetry of heavy-ion beams

In a similar way the results of the experiment confirm the polarization correlations predicted for radiative recombination [74]. They lead to a unique method of heavy-ion beam polarimetry. It should work in the specific case of polarized hydrogenlike ions. Such a method is currently demanded for near future experiments with stored beams. A measurement of parity nonconservation and a test of the standard model of elementary particles and interactions [81,82] is one of the possible examples of such experiments.

C. Circular γ -ray polarimetry

Recently a method of imaging γ -ray polarimetry was proposed which is sensitive to circular polarization of γ quanta [83]. This method relies on production of polarized Compton-recoiled electrons by circularly polarized photons and production of bremsstrahlung by these electrons. The angular distribution and linear polarization of bremsstrahlung are directly related to circular polarization of the incoming photons. Detailed understanding of bremsstrahlung polarization correlations is mandatory for the realization of this technique.

D. Measurement of g factors

Since the spin rotation is sensitive to the scattered particle g factor [see Eq. (22)], the latter can be extracted from the measurement. Our classical model is valid for every spinning charged particle, for example for a nucleus. Both the spin of the scattered nucleus and the orbital momentum of the coupled system rotate during the scattering process. Therefore nucleus-nucleus scattering or nucleus-nucleus bremsstrahlung can be used to measure g factors. In both cases one needs to use a bare ion beam polarized within the scattering plane. Then in the first case the nuclear spin orientation after the scattering should be identified. In the second case the linear polarization of the nucleus-nucleus bremsstrahlung should be

measured. From any of these measurements the spin rotation can be determined, which is related to the g factor.

In particular this may be useful for radioactive ion beams. Such beams are produced by fragmentation, fusion-evaporation, or fission reactions with fast initially stable beams. Such reactions produce transversely polarized exotic nuclei, which are thus prepared for the measurement.

X. CONCLUSIONS

We have optimized the technique of hard x-ray Compton polarimetry and significantly improved its efficiency and angular resolution. The angular resolution of $\sigma = 0.3^\circ$ is a significant achievement of Compton polarimetry. With this we were sensitive to the bremsstrahlung polarization correlations $P_2(1,0,0)$ and $P_2(0,0,1)$. In this experiment we measured two correlation parameters $\frac{C_{31}}{C_{03}} = \frac{P_2(0,0,1)}{P_1(0,0,0)}$ and $\frac{C_{11}}{C_{03}} = -\frac{P_2(1,0,0)}{P_1(0,0,0)}$. The results are in excellent agreement with fully relativistic calculations.

A simple classical model qualitatively explains the observed phenomena. It indicates that the electron scattering geometry is not confined to a single plane. Such an observation is typically not possible in scattering experiments.

A setup of one photon linear polarimeter and four conventional photon detectors allows determination of all three components of the electron spin. This electron polarimetry method can be applied in the energy range of 100 keV up to several 10 MeV.

In a similar way the experiment confirms the theoretical predictions for the polarization correlations in radiative recombination. They lead to the unique method of polarimetry of heavy-ion beams.

ACKNOWLEDGMENTS

This work was supported by the German Research Foundation (DFG) within the Emmy Noether program under Contract No. TA 740 1-1; by the Swedish Research Council, Contract No. 2007-4067; and by the Göran Gustafsson Foundation. The Darmstadt group acknowledges financial support by DFG through SFB 634 and by the state of Hesse through the Helmholtz International Center for FAIR within the LOEWE program. A.S. acknowledges support by the Helmholtz association under Project No. VH-NG-421. We are grateful to P. Amaro for deriving Eq. (26) and to G. Weber for his comments.

-
- [1] J. W. Motz and R. C. Placious, *Phys. Rev.* **109**, 235 (1958).
 [2] H. W. Koch and J. W. Motz, *Rev. Mod. Phys.* **31**, 920 (1959).
 [3] H. E. Hall, A. O. Hanson, and D. Jamnik, *Phys. Rev.* **129**, 2207 (1963).
 [4] G. Elwert and E. Haug, *Phys. Rev.* **183**, 91 (1969).
 [5] B. Starek, H. Aiginger, and E. Unfried, *Phys. Lett. A* **39**, 151 (1972).
 [6] R. H. Pratt and H. K. Tseng, *Phys. Rev. A* **11**, 1797 (1975).
 [7] H. K. Tseng, R. H. Pratt, and C. M. Lee, *Phys. Rev. A* **19**, 187 (1979).
 [8] R. H. Pratt, H. K. Tseng, C. M. Lee, and L. Kissel, *At. Data Nucl. Data Tables* **20**, 175 (1977).
 [9] L. Kissel, C. A. Quarles, and R. H. Pratt, *At. Data Nucl. Data Tables* **28**, 381 (1983).
 [10] S. M. Seltzer and M. J. Berger, *At. Data Nucl. Data Tables* **35**, 345 (1986).
 [11] R. Hippler, K. Saeed, I. McGregor, and H. Kleinpoppen, *Phys. Rev. Lett.* **46**, 1622 (1981).
 [12] M. Semaan and C. Quarles, *Phys. Rev. A* **26**, 3152 (1982).
 [13] S. Portillo and C. A. Quarles, *Phys. Rev. Lett.* **91**, 173201 (2003).
 [14] R. L. Gluckstern, M. H. Hull, Jr., and G. Breit, *Phys. Rev.* **90**, 1026 (1953).
 [15] H. Olsen and L. C. Maximon, *Phys. Rev.* **110**, 589 (1958); **114**, 887 (1959).
 [16] E. Haug, *Phys. Rev.* **188**, 63 (1969).
 [17] H. K. Tseng and R. H. Pratt, *Phys. Rev. A* **3**, 100 (1971).
 [18] J. W. Motz, *Phys. Rev.* **104**, 557 (1956).
 [19] J. W. Motz and R. C. Placious, *Phys. Rev.* **112**, 1039 (1958); *Nuovo Cimento* **15**, 571 (1960).
 [20] R. W. Kuckuck and P. J. Elbert, *Phys. Rev. A* **7**, 456 (1973).
 [21] W. Lichtenberg, A. Przybylski, and M. Scheer, *Phys. Rev. A* **11**, 480 (1975).
 [22] S. Tashenov, T. Bäck, R. Barday, B. Cederwall, J. Enders, A. Khaplanov, Y. Poltoratska, K. U. Schässburger, and A. Surzhykov, *Phys. Rev. Lett.* **107**, 173201 (2011).
 [23] R. Märtin *et al.*, *Phys. Rev. Lett.* **108**, 264801 (2012).
 [24] N. Sherman, *Phys. Rev.* **103**, 1601 (1956).
 [25] J. W. Motz, H. Olsen, and H. W. Koch, *Rev. Mod. Phys.* **36**, 881 (1964).
 [26] S. C. Miller and R. M. Wilcox, *Phys. Rev.* **124**, 637 (1961).
 [27] W. R. Johnson and J. D. Rozics, *Phys. Rev.* **128**, 192 (1962); J. D. Rozics and W. R. Johnson, *ibid.* **135**, B56 (1964).
 [28] E. S. Sobolak and P. Stehle, *Phys. Rev.* **129**, 403 (1963).
 [29] E. Haug, *Z. Phys. D* **37**, 9 (1996).
 [30] A. P. Potylitsyn, *Eur. Phys. J. C* **70**, 107 (2010).
 [31] K. GÜthner, *Z. Phys.* **182**, 278 (1965).
 [32] A. Aehlig, *Z. Phys. A* **294**, 291 (1980).
 [33] H. A. Schaefer, W. Drachenfels, and W. Paul, *Z. Phys. A* **305**, 213 (1982).
 [34] E. Mergl and W. Nakel, *Z. Phys. D* **17**, 271 (1990).
 [35] E. Geisenhofer and W. Nakel, *Z. Phys. D* **37**, 123 (1996).
 [36] E. Mergl, H.-Th. Prinz, C. D. Schröter, and W. Nakel, *Phys. Rev. Lett.* **69**, 901 (1992).
 [37] C. D. Shaffer, X.-M. Tong, and R. H. Pratt, *Phys. Rev. A* **53**, 4158 (1996).
 [38] M. Nofal *et al.*, *Phys. Rev. Lett.* **99**, 163201 (2007).
 [39] H.-H. Behncke and W. Nakel, *Phys. Rev. A* **17**, 1679 (1978).
 [40] W. Bleier and W. Nakel, *Phys. Rev. A* **30**, 607 (1984); **30**, 661 (1984).
 [41] K. W. McVoy and U. Fano, *Phys. Rev.* **116**, 1168 (1959).
 [42] R. H. Pratt, *Phys. Rev.* **120**, 1717 (1960).
 [43] I. J. Feng, I. B. Goldberg, Y. S. Kim, and R. H. Pratt, *Phys. Rev. A* **28**, 609 (1983).
 [44] U. Fano, *Phys. Rev.* **178**, 131 (1969).

- [45] C. Fronsdal and H. Überall, *Phys. Rev.* **111**, 580 (1958).
- [46] H. K. Tseng and R. H. Pratt, *Phys. Rev. A* **7**, 1502 (1973).
- [47] D. H. Jakubassa-Amundsen, *Phys. Rev. A* **82**, 042714 (2010).
- [48] V. A. Yerokhin and A. Surzhykov, *Phys. Rev. A* **82**, 062702 (2010).
- [49] D. H. Jakubassa-Amundsen and A. Surzhykov, *Eur. Phys. J. D* **62**, 177 (2011).
- [50] V. Balashov, A. Grum–Grzhimailo, and N. Kabachnik, *Polarization and Correlation Phenomena in Atomic Collisions* (Kluwer Academic/Plenum, New York, 2000).
- [51] Y. Poltoratska *et al.*, in *Spin Physics: 18th International Spin Physics Symposium*, edited by D. G. Crabb, Y. Prok, M. Poelker, S. Liuti, D. B. Day, and X. Zheng, AIP Conf. Proc. No. 1149 (AIP, New York, 2009), p. 983.
- [52] T. J. Gay and F. B. Dunning, *Rev. Sci. Instrum.* **63**, 1635 (1992).
- [53] G. B. Dunning, *Nucl. Instrum. Methods Phys. Res., Sect. A* **347**, 152 (1994).
- [54] M. Salomaa and H. A. Enge, *Nucl. Instrum. Methods* **145**, 279 (1977).
- [55] F. Metzger and M. Deutsch, *Phys. Rev.* **78**, 551 (1950).
- [56] S. Tashenov *et al.*, *Nucl. Instrum. Methods Phys. Res., Sect. A* **600**, 599 (2009).
- [57] S. Agostinelli *et al.*, *Nucl. Instrum. Methods Phys. Res., Sect. A* **506**, 250 (2003).
- [58] S. Chauvie *et al.*, *IEEE Nucl. Sci. Symp. Conf. Rec.* **3**, 1881 (2004).
- [59] S. Tashenov *et al.*, *Phys. Rev. Lett.* **97**, 223202 (2006).
- [60] G. Weber *et al.*, *Phys. Rev. Lett.* **105**, 243002 (2010).
- [61] C. A. Quarles, *Radiat. Phys. Chem.* **59**, 159 (2000).
- [62] ICRU Report No. 37, 1984 (unpublished).
- [63] G. Weber *et al.*, *Nucl. Instrum. Methods Phys. Res., Sect. B* **279**, 155 (2012).
- [64] J. D Callen, <http://homepages.cae.wisc.edu/~callen/book.html>
- [65] L. Kim and R. H. Pratt, *Phys. Rev. A* **36**, 45 (1987).
- [66] L. H. Thomas, *Nature (London)* **117**, 514 (1926); *Philos. Mag. Ser. 7* **3**, 122 (1927).
- [67] V. Bargmann, L. Michel, and V. L. Telegdi, *Phys. Rev. Lett.* **2**, 435 (1959).
- [68] F. A. Berezin and M. S. Marinov, *Ann. Phys. (NY)* **104**, 336 (1997).
- [69] V. I. Kozoriz and Yu. R. Musin, *Theor. Math. Phys.* **123**, 467 (2000).
- [70] J. Jackson, *Classical Electrodynamics* (John Wiley & Sons, New York, 1998).
- [71] R. J. Van Duinen and J. W. G. Aalders, *Nucl. Phys. A* **115**, 353 (1968).
- [72] J. Eichler and Th. Stöhlker, *Phys. Rep.* **439**, 1 (2007).
- [73] A. Surzhykov, S. Fritzsche, Th. Stöhlker, and S. Tachenov, *Phys. Rev. A* **68**, 022710 (2003).
- [74] A. Surzhykov, S. Fritzsche, Th. Stöhlker, and S. Tashenov, *Phys. Rev. Lett.* **94**, 203202 (2005).
- [75] S. Fritzsche, A. Surzhykov, and Th. Stöhlker, *Phys. Rev. A* **72**, 012704 (2005).
- [76] A. Bisi and L. Zappa, *Phys. Rev. Lett.* **1**, 332 (1958).
- [77] S. Galster and H. Schopper, *Phys. Rev. Lett.* **4**, 295 (1960).
- [78] S. Tashenov and J. Gerl, *Nucl. Instrum. Methods Phys. Res., Sect. A* **586**, 224 (2007).
- [79] S. Tashenov and J. Gerl, *Nucl. Instrum. Methods Phys. Res., Sect. A* **622**, 592 (2010).
- [80] R. H. Pratt *et al.*, *Phys. Rev.* **134**, A916 (1964).
- [81] L. N. Labzowsky, A. V. Nefiodov, G. Plunien, G. Soff, R. Marrus, and D. Liesen, *Phys. Rev. A* **63**, 054105 (2001).
- [82] A. V. Nefiodov *et al.*, *Phys. Lett. B* **534**, 52 (2002).
- [83] S. Tashenov, *Nucl. Instrum. Methods Phys. Res., Sect. A* **640**, 164 (2011).